The importance of electronic correlations in exploring the exotic phase diagram of layered Li_xMnO_2

Hrishit Banerjee,[1, 2, 3, *] Clare P. Grey,[1, 3] and Andrew J. Morris[2, 3, †]

[1] *Yusuf Hamied Department of Chemistry, University of Cambridge, Lensfield Road, CB2 1EW, Cambridge, UK.*
[2] *School of Metallurgy and Materials, University of Birmingham, Elms Road, B15 2TT, Edgbaston, Birmingham, UK.*
[3] *The Faraday Institution, Quad One, Becquerel Avenue, Harwell Campus, Didcot, OX11 0RA, UK*

(Dated: April 14, 2023)

Using *ab initio* dynamical mean-field theory we explore the electronic and magnetic states of layered Li_xMnO_2 as a function of x, the state of charge. Constructing real-space Wannier projections of Kohn-Sham orbitals based on the low-energy subspace of Mn 3*d* states and solving a multi-impurity problem, our approach focuses on local correlations at Mn sites. The antiferromagnetic insulating state in $LiMnO_2$ has a moderate Néel temperature of $T_N = 296\,K$ in agreement with experimental studies. Upon delithiation the system proceeds through a number of states: ferrimagnetic correlated metals at x=0.92, 0.83; multiple charge disproportionated ferromagnetic correlated metals with large quasiparticle weights at x=0.67, 0.50, 0.33; ferromagnetic metals with small quasiparticle weights at x=0.17, 0.08 and an antiferromagnetic insulator for the fully delithiated state, $x = 0.0$. At moderate states of charge, $x = 0.67 - 0.33$, a mix of +3/+4 formal oxidation states of Mn is observed, while the overall nominal oxidation of Mn state changes from +3 in $LiMnO_2$ to +4 in MnO_2. In all these cases the high-spin state emerges as the most likely state in our calculations considering the full *d* manifold of Mn based on the proximity of e_g levels in energy to t_{2g}. The quasiparticle peaks in the correlated metallic states were attributed to polaronic states, based on previous literature for similar isoelectronic JT driven materials, arising due to non-Fermi liquid type behaviour of the strongly correlated system.

Introduction $LiMnO_2$ (LMO) [1–3] has the potential to be a low-cost, low-toxicity, high safety, and environmentally friendly alternative to the most popular rechargeable lithium-ion battery cathode material, $LiCoO_2$[1, 4–8], however at 50 % delithiation LMO irreversibly transforms to a spinel ($Fd\bar{3}m$) phase, which causes significant reduction in the capacity and operating voltage, limiting its large-scale application [9–11].

The thermodynamically stable phase of LMO at ambient conditions is orthorhombic (Pmmn) [12] although a rhombohedral layered O3 structure, may be produced by ion exchange from $NaMnO_2$[1, 2]. The rhombohedral O3 structures comprise a family of materials, including $LiCoO_2$ (LCO), $LiNiO_2$ (LNO) [13–15] and $LiNi_{1-x-y}Mn_yCo_xO_2$ (NMC) [8, 16–21]. Within this family LMO adopts the same oxygen stacking as LCO, but with symmetry reduced from rhombohedral ($R\bar{3}m$) to monoclinic (C2/m), as a result of a cooperative Jahn-Teller(JT) distortion. Based on magnetization data [12, 22] pristine monclinic LMO is an antiferromagnetic insulator in its high spin state with relatively moderate Neél temperatures ($T_N \sim 250\,K$) due to the stabilisation of antiferromagnetism by the cooperative JT distortions [22].

Structural phase transitions during cycling have prevented the widespread adoption of layered monoclinic LMO as a cathode material. Upon 50% delithiation, layered phase to spinel structural phase transformation of LMO involves the migration of Mn ions, whilst the close-packed O lattice remains intact. Density-functional theory (DFT) calculations, combined with a hybrid eigenvector-following method to uncover the pathways, show that for the case of $x = 0.5$, particular orderings of Li^+/Li^+ vacancy and Mn^{3+}/Mn^{4+} ions play a significant role in this structural transformation [1, 9, 23–26]. Moreover the ionic pathways that give rise to the ordering and transformations are highly dependent on the inclusion of a Hubbard U term in the Kohn-Sham Hamiltonian, hinting that these structural changes may have a strong underlying electronic origin. However, the role of electron correlations in the origin of the mixed-valence charge-ordered state, as well as the possibility of existence of such states at other states-of-charge remains unknown.

Electronic phase transitions occurring during cathode cycling[27–32] significantly influence the reversibility of the (de)lithiation process, in terms of rate limiting formation and propagation of phase boundaries, lattice mismatch and volume changes, all of which lead to slow (de)lithiation kinetics hence affecting rate capability and stability, causing degradation of the active material [33]. For example, a first-order metal-insulator transition, normally driven through doping [34, 35] or pressure [36, 37], is driven electronically in Li_xCoO_2 as a function of states-of-charge x [30–32]. Naturally the question arises whether such a electrochemically driven metal-insulator transition, or other exotic phases may also be observed in the analogous cathode material LMO.

Electrochemical and magnetic phase transition studies of complex layered oxides are made all the more robust through first principles modelling of the electronic and magnetic states of these materials. Whilst the first order metal-insulator transition observed in LCO has been

postulated to be a Mott transition by some DFT studies [31, 38], a true Mott transition is difficult to capture within non-interacting DFT and warrants the use of many body methods like dynamical mean-field theory (DMFT) [39–44]. Recently a DFT + DMFT study to account for both static and dynamic correlations has been carried out to explore this Mott transition and associated compositional phase diagram in Li_xCoO_2 [45]. Here local interactions, which DMFT describes, are seen to strongly impact self energies, occupancies of d orbitals, phase stability and electronic behaviour of LCO at various x. Pristine LCO is an insulator while delithiated phases are moderately correlated Fermi liquids with modest quasiparticle weights. Quasiparticles like polarons are known to affect charge conductivity in batteries [46, 47]. It is likely that similar treatment of strong correlations is essential for modelling plausible phase transitions in LMO.

One of the main bottlenecks to the use of DMFT in battery cathodes is that they need to be studied at different states-of-charge. This means dealing with multiple inequivalent sites, and hence solving multi-impurity problems. This has the disadvantage of having to solve very large density matrices which are not only very expensive, but may often have large off diagonal terms, leading to fermionic sign problems.

In this letter we predict using DFT+DMFT the phase transitions in layered monoclinic Li_xMnO_2, as a function of x, and explore the temperature versus x phase diagram. We develop a computationally fast method to deal with multi-impurity DMFT calculations. The electronic and magnetic state of pristine LMO are examined and compared to experimental results at temperatures below and above T_N. The system is then delithiated systematically and for each x we present the spectral functions, magnetic properties, and transition temperatures. We find a metal-insulator Mott transition as a function of delithiation and the emergence of exotic states like ferrimagnetic correlated metals with large quasiparticle weights and charge-ordered ferromagnetic correlated metals with large quasiparticle peaks arising due to non-Fermi liquid behaviour shown by polarons. We clarify that origin of the charge disproportionated mixed valence states is due to different quasiparticle weights at different sites and postulate this ordering to be present for a range of x. The pathways leading to structural transformations to spinel structure could be traced back to such charge disproportionated state.

Computational Methodology We develop a method to carry out multi-impurity DMFT calculations in a novel way by mapping multi-impurity problems to equivalent number of single-impurity problems interacting through bath hybridisation by means of Wannier projections. Delithiating the system results in formation of crystallographically inequivalent Mn sites in the LMO supercell, which requires solving multi-impurity problems, involving solution of extremely large density matrices, which is computationally expensive, and has fermionic sign problem at low temperatures. To make the problem tractable, Maximally Localised Wannier Functions (MLWF) were constructed for all structurally inequivalent sites, however each inequivalent site was solved as a single-impurity problem interacting through the bath with the other inequivalent sites by virtue of the constructed MWLF, and the bath hybridisation. This method works well for strongly localised systems and makes accurate calculations at low temperatures converge faster with much less noise, avoiding the fermionic sign problem. Further details on parameters and comparison to conventional DMFT cf. SI

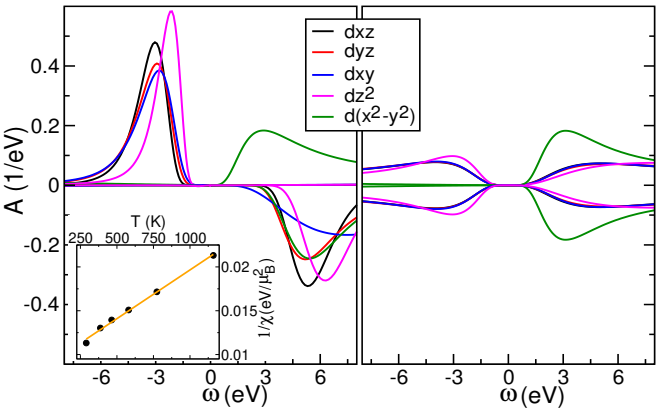

FIG. 1: The DMFT spectral functions and magnetic calculations in LMO. Figure shows the DMFT spectral functions for both single-site spin-polarised (at T=58 K, left panel) and paramagnetic (at T=580 K, right panel) calculations. Inset in left panel shows the plot of $1/\chi$ vs temperature on application of small magnetic fields at various temperatures. The straight line Curie-Weiss fit χ=C/(T-θ) for the data is shown.

Results To correctly account for dynamic correlation effects on Mn d states, we first carry out single-impurity DMFT calculations for Mn d based low-energy Hamiltonians defined in the basis of DFT-derived Wannier functions (cf. SI).

The paramagnetic state of pristine layered monoclinic LMO at T=580K shown by the paramagnetic spectral function in Fig. 1 (a) (right) shows good agreement with XPS spectral line-shapes in experimental studies [48]. Pristine LMO is an insulator [22, 49] however experimental value of the electronic band gap is unknown. A wide range of band gap values from 0.3 eV to 1.8 eV have been reported from *ab initio* calculations based on various choices of static Hubbard U in DFT+U calculations[49–53]. We report a paramagnetic band gap of ∼0.6eV, with $U' = 5eV$. We find 3 slightly degeneracy broken t_{2g} states that are half-filled, 1 e_g state is half-filled and 1 e_g state completely empty. The impurity charge on Mn is 3.99 $|e|$ indicating Mn is in a d^4 (+3) formal oxidation state, again in agreement with XPS experiments [48].

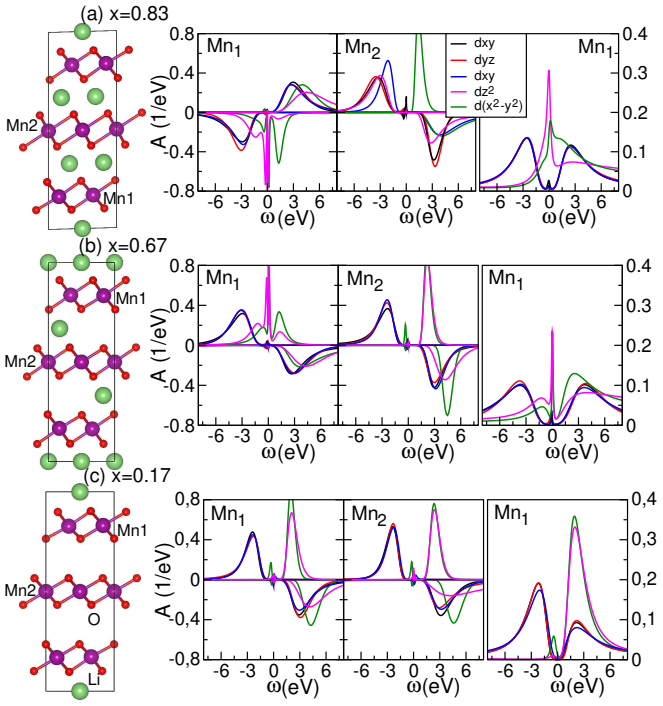

FIG. 2: The structures and orbital resolved DMFT spectral functions for various states of charge showing the various phases as a function of x. The orbital spectral functions are denoted by the same colours as in Figure 1. (a) shows the case of $x = 0.83$. The top far right panel shows the paramagnetic spectral function for Mn_1. (b) shows the case of $x = 0.67$. The middle far right panel shows the paramagnetic spectral function for Mn_1. (c) shows the case for $x = 0.17$. The bottom far right panel shows the paramagnetic spectral function ofr Mn_1.

Next, we proceed to explore the magnetism within single-impurity DMFT. For this purpose, we start from the paramagnetic solutions, add a symmetry breaking term in form of a spin-splitting term in the real part of the self energies, and let the DMFT iterative cycle converge to a possible symmetry-broken solution with net ordered magnetic moment. We carry out the calculations at various different values of inverse temperature with β between 20 and 300 eV^{-1}, where $\beta = \frac{1}{k_B T}$, where k_B is the Boltzmann's constant. At $\beta = 20\,\mathrm{eV}^{-1}$ ($T = 580\,K$), the calculations are found to converge to a paramagnetic state, while upon reducing temperature, a transition to a magnetic solution is found. In Fig.(SI) 2 , we show a plot of the ordered average Wannier moments of Mn Wannier functions with the number of DMFT iterations. The ordered moments (saturating around $3.25\,\mu_B$) are not stable, they oscillate as a function of iteration. This shows the propensity of the system towards antiferromagnetic fluctuations being present in the system [54]. The spectral function for the magnetic state shows insulating behaviour. The ordered saturation moment and antiferromagnetic behaviour is in good agreement with susceptibility experiments [22].

Using a $U' = 5\,eV$ within DMFT the antiferromagnetic band gap is ∼1.2 eV.

In order to determine the Néel temperature (T_N) we carry out susceptibility calculations with an external field applied on the system. We vary the applied field from $0.01 - 0.03$ eV in steps of 0.01 eV, and for each value of temperature we obtain the inverse slope of the magnetisation vs applied field within the linear regime. Magnetic fields are applied as a split in energy and the value of magnetic field is added to the DFT Hamiltonian. The contribution $-h_{\mathrm{field}} \times \Sigma$ is added to diagonal elements of the Hamiltonian. This gives the inverse of the uniform susceptibility $1/\chi$ vs temperature T, as shown in Fig.1 (b). By fitting the data to Curie Weiss law χ=C/(T-θ), where C is Curie constant, θ is Weiss temperature in the high temperature regime we find $\theta = 769\,K$ in excellent agreement with experimentally reported values on two different samples $\theta = 790\,K,\ 540\,K$, [22] and a calculated value of $\theta = 790\,K$ [52]. This has been attributed to the stabilisation of antiferromagnetic state due to the cooperative JT distortion [52]. The calculated Néel temperature (T_N) ∼296K, is also in agreement with experiments [22]. We use the same set of parameters throughout for benchmarking of T_N with experimental data.

Next we look at delithiating the pristine LMO by making two supercells of dimensions $3 \times 1 \times 1$ and $3 \times 2 \times 1$. This results in 6 and 12 symmetry equivalent Mn sites in case of $3 \times 1 \times 1$ and $3 \times 2 \times 1$ respectively. One Li atom is removed sequentially at each stage and various resulting structures are relaxed within DFT using the PBESol exchange-correlation functional. For the sake of brevity we do not enumerate all the structural details here however a significant contraction of lattice parameters and lattice volume is seen on delithiation, as also observed in experiments, as well as a reduction in JT distortion in the system is observed. The various fractions of x considered here are $x = 0.92, 0.83, 0.67, 0.50, 0.33, 0.17, 0.08,$ and 0.00. However, $x = 0.00$ is an extreme case: removing all the Li from the structure is not possible experimentally and makes the structure unstable.

In case of delithiation to $x = 0.83$, the 6 symmetry equivalent Mn atoms in the pristine $3 \times 1 \times 1$ cell are now split by reduction of symmetry into have 4 structurally inequivalent types, Mn_1, Mn_2, Mn_3 and Mn_4 each with multiplicity 2, 1, 2 and 1 respectively. We find a ferrimagnetic state in this case since from the DMFT spectral functions and from magnetic moments in Table 1 (SI) we see that Mn_1 with multiplicity=2 (Mn_3 spectral function is electronically similar to Mn_1) is oppositely oriented to Mn_2 with multiplicity=1 (Mn_4 spectral function is electronically similar Mn_2), as shown in Fig. 2 (a). A large quasiparticle peak is seen at the chemical potential in Mn_1 and Mn_3 indicating a strongly correlated metallic state[44]. Thus these 4 structurally inequivalent types may thus be primarily be grouped into two

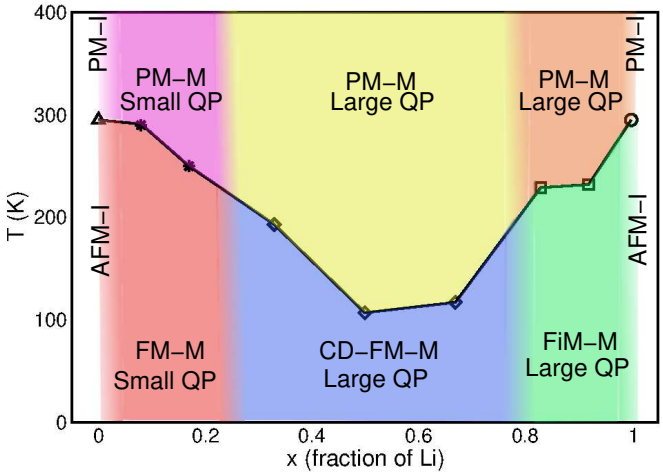

FIG. 3: The different phases at different temperatures of Li_xMnO_2 as a function of Li content. Where AFM-I refers to antiferromagnetic insulator; FiM-M, ferrimagnetic metal; FM-M, ferromagnetic metal; PM-I, paramagnetic insulator; PM-M, paramagnetic metal; CD, charge disproportionated; and QP, quasiparticle. The different symbols on the line corresponds to the actual data points demarcating the different phases.

categories - one with large quasiparticle and the other with small quasiparticle weights. This quasiparticle peak have a polaronic nature as suggested by previous studies on isoelectronic JT active manganites [55, 56]. The spectral function for the $x = 0.83$ filling is orbital resolved and shows that the t_{2g} orbitals are partially filled and one of the e_g orbitals is partially filled while the other e_g orbital is empty, as shown in Fig 2(a). This implies an occupancy of d^4 and a formal oxidation state of +3. The occupancies and Wannier moments are given in Table 1 (SI). The paramagnetic phase at T=580 K corresponds to a strongly correlated paramagnetic metal with a large quasiparticle peak and non-Fermi liquid behaviour as seen from the paramagnetic spectral function shown in the top right panel of Fig 2 (a). The electronic structure for the case of $x = 0.92$ is found to be very similar to $x = 0.83$.

Delithiated states with $x = 0.67, 0.50, 0.33$ show similar electronic structure to each other across this range of x with certain slight differences, and belong to the same phase of charge-ordered ferromagnetic correlated metallic states. In case of $x = 0.67$ and $x = 0.33$, the 6 symmetry equivalent Mn atoms in the pristine $3 \times 1 \times 1$ cell are again split by reduction of symmetry into 4 structurally inequivalent types, Mn_1, Mn_2, Mn_3 and Mn_4, each with different multiplicities of 2, 1, 2, 1 respectively, however in case of $x = 0.50$ there are 2 structurally inequivalent sites each with multiplicity 3. These sites may primarily be grouped again into two categories - one group with large quasiparticle and the other group with small quasiparticle weights. The $x = 0.67$ state is ferromagnetic since all Mn sites have the same orientation in the spectral function, as shown in Fig. 2 (b), and can also be seen from Moments in Table 1 (SI). A large quasiparticle peak is seen at the chemical potential in Mn_1 (multiplicity=2), Mn_3(multiplicity=2) and Mn_4 (multiplicity=1). Mn_3 and Mn_4 not shown here for the sake of brevity. The middle right panel of Fig. 2 shows the paramagnetic spectral function as a strongly correlated metal for Mn_1, for the case of $x = 0.67$. Large quasiparticle weights are also seen on Mn_1, with multiplicity of 3 (for $x = 0.50$) and on Mn_1 with multiplicity 2 for $x = 0.33$, indicating a strongly correlated metallic state in all cases. From Table 1 (SI) a mix of +3 and +4 states are seen in all these cases of $x = 0.67, 0.50, 0.33$ with different fractions of +3 and +4 Mn being present in the system. It is also seen from the spectral functions that this mixed oxidation state and corresponding charge disproportionation originates due to different quasiparticle weights on different sites. Spectral functions obtained for $x = 0.50$, and 0.33 are seen to be qualitatively similar to the case of $x = 0.67$.

In case of the delithiated state with $x = 0.17$ the 6 symmetry equivalent Mn atoms in the pristine $3 \times 1 \times 1$ cell are also split by reduction of symmetry into 4 structurally inequivalent types, Mn_1, Mn_2, Mn_3 and Mn_4 each with multiplicity 2, 1, 2 and 1 respectively. Qualitatively all Mn have similar electronic structures at all sites. A ferromagnetic arrangement is observed here since all Mn sites have same orientation as can be seen from the spectral function in fig. 2 (c) as well as in Table 1 (SI). A small quasiparticle peak is seen at the chemical potential in each of Mn_1, Mn_2 and Mn_3 indicating a moderately correlated metallic state. A majority of +4 oxidation states are seen. There is no charge disproportionation/ordering in this case. The bottom right panel 2 (c) shows the paramagnetic weakly correlated metallic state with a small quasiparticle peak. Similar spectral functions and magnetic structures are obtained in case of $x = 0.08$.

Discussion The exotic phase diagram and associated phase transitions in Li_xMnO_2 as a function of x vs temperature, is shown in Fig 3. The y axis shows the phase change from magnetic to paramagnetic states at each x driven by competition of thermal fluctuations with magnetic order. The change of magnetic phases along x is more nuanced. JT distorted materials show large superexchange which favours anti-ferromagnetism. This is the case of the pristine material $x = 1$, which is a JT driven antiferromagnetic insulator. As the system is delithiated, JT distortion reduces on different MnO_6 octahedra, which in turn indicates a reduction in monoclinicity. This reduction in JT favours ferromagnetism instead of anti-ferromagnetism. At $x = 0.83$ there are few sites with reduced JT distortion and hence ferromagnetic exchange whereas majority of other sites still have significant JT distortion and hence show Mn-Mn antiferromagnetic superexchange, leading to an overall ferri-

magnetic state. When further delithiated to $x = 0.67$, and beyond, the overall reduction of JT distortion now favours FM double exchange, between different occupancies at majority of Mn sites. Reduction in JT distortion is usually associated with ferromagnetism particularly in Manganites [57–59].

To elucidate the origin of polaronic quasiparticles on delithiating we look at the crossover from coherence (Fermi-liquid) to incoherence (non-Fermi liquid) behaviour as a function of x. We plot $-Im\Sigma(\omega \to 0)$, Σ is self energy, as a function of x shown in Fig. 4 which gives the measure of the coherence/incoherence behaviour of the quasiparticle states [54]. A finite value of this quantity indicates a strongly correlated incoherent state - such as a polaron in this case, which is indicative of non-Fermi liquid behaviour, in ground state, not captured by DFT. This manifests as a large localised peak in the spectral function obtained from interacting Green's functions, which is known as a quasiparticle peak. Large quasiparticle polaronic states arise on delithiation on some Mn sites owing to non-Fermi liquid behaviour of the system. Charge disproportionation into Mn^{3+}/Mn^{4+} states result from large quasiparticles on some sites and small quasiparticles on others. $-Im\Sigma(\omega \to 0)$ is shown for the site with largest quasiparticle weights seen in spectral functions. As we show an increase in incoherent or non-Fermi liquid type behaviour is seen with delithiation from x=0.83 to x=0.33, which indicates that these are strongly correlated quasiparticle states, and explains the origin of the polaronic states. Doped manganites in general have been known to show polaronic quasiparticle peaks[56].

Conclusion In summary we have shown the exotic phase diagram and phase transitions in Li_xMnO_2 as a function of state-of-charge x, and temperature. Our study shows a novel method of carrying out multi-impurity DMFT calculations in cathode materials in a computationally tractable way, thus opening up the field of battery physics in terms of strong correlations based many-body studies. It demonstrates an electrochemical method of tuning strongly correlated phase transitions and also shows emergence of polaronic quasiparticle states which contribute to charge disproportionation and which eventually lead to structural transformations seen in this material, and helps us in understanding degradation in cathodes.

We find that an antiferromagnetic insulating state emerges in $LiMnO_2$, with a Weiss temperature of $\theta = 769\,K$, in its +3 formal oxidation state, in high-spin configuration, in excellent agreement with experimental measurements. As the system is delithiated at fractions of $x = 0.92$, and 0.83 we predict a ferrimagnetic correlated metallic state thus observing a metal-insulator transition, similar to that in LCO. From the DMFT spectral function this metal-insulator transition is seen to be of a Mott type transition with a large quasiparticle weight in the strongly correlated metallic state.

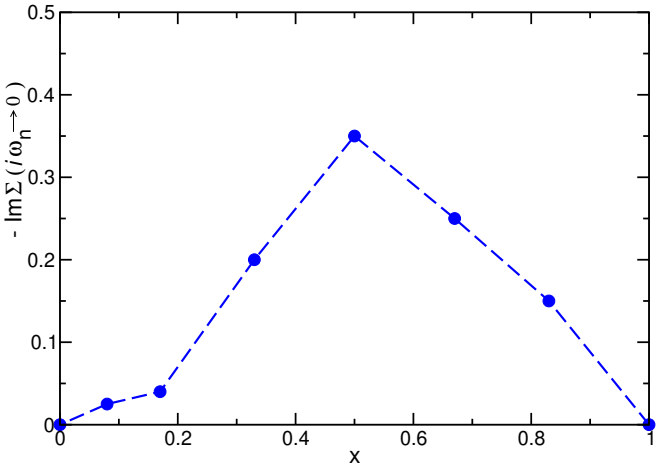

FIG. 4: Figure showing the plot of -Im Σ ($\omega \to 0$) which gives a measure of coherence/incoherence behaviour as a function of state of charge plotted for the sites with largest quasiparticle weights. A finite value of this quantity indicates a strongly correlated non-Fermi liquid type metallic behaviour with a large quasiparticle weight indicating the presence of large polarons. An infinitesimally small value tends to indicate a weakly correlated coherent Fermi liquid type behaviour.

At fractions of $x = 0.67, 0.5$, and 0.33 we find the system to be in ferromagnetic strongly correlated metallic state with a mix of +3/+4 formal oxidation states. The pathways leading to the structural transformation to low energy spinel structure, originates with orderings of Li^+/Li_{vac} and $Mn^{3+}/\ Mn^{4+}$ mixed oxidation states at $x = 0.50$ [9]. We postulate that this $Mn^{3+}/\ Mn^{4+}$ charge disproportionation occurs due to the different quasiparticle weights at different sites.

At a high state of charge with $x = 0.17$, we find a ferromagnetic correlated metal with a small quasiparticle peak near a formal oxidation state of +4.

An overall nominal oxidation state change of Mn from +3 in $LiMnO_2$ to +4 in MnO_2 is observed, through stages of mixed oxidation states. In all these cases the high-spin state emerges as the most likely state considering the full d manifold of Mn in the model.

The quasiparticle peaks in the correlated metallic states were attributed to polaronic states, owing to incoherent non-Fermi liquid behaviour, and the correlated metallic systems may be thought of as polaronic hopping semiconductors.

Our novel and faster method of carrying out multi-impurity DMFT calculations involves calculating Wannier projections for all impurities and solving each separately keeping others in the bath, interacting through the bath hybridisation.

To the best of our knowledge a systematic examination of the electrochemically driven Mott transition and the full phase diagram of LMO from a correlations based

perspective does not exist, nor does an explanation for the observed orbital ordering at $x = 0.50$ and our study is expected to give rise to further experimental studies exploring these aspects of this very important cathode material through possible *in-situ* XPS+BIS spectra and magnetic susceptibility measurements while charging and discharging of the LMO cathodes.

The authors acknowledge fruitful discussion with Annalena R. Genreith-Schriever. This work has been funded by the Faraday Institution degradation project (FIRG001, FIRG024). Calculations have been performed on the odyssey cluster, the CSD3 cluster of the University of Cambridge. Generous computing resources were provided by the Sulis HPC service (EP/T022108/1), and networking support by CCP-NC (EP/T026642/1), CCP9 (EP/T026375/1), and UKCP (EP/P022561/1).

* Electronic address: hb595@cam.ac.uk
† Electronic address: a.j.morris.1@bham.ac.uk

[1] A. R. Armstrong and P. G. Bruce, Nature **381**, 499 (1996), ISSN 1476-4687, URL https://doi.org/10.1038/381499a0.

[2] F. Capitaine, P. Gravereau, and C. Delmas, Solid State Ionics **89**, 197 (1996), ISSN 0167-2738, URL https://www.sciencedirect.com/science/article/pii/0167273896003694.

[3] G. Vitins and K. West, Journal of The Electrochemical Society **144**, 2587 (1997), URL https://doi.org/10.1149/1.1837869.

[4] M. Thackeray, W. David, P. Bruce, and J. Goodenough, Materials Research Bulletin **18**, 461 (1983), ISSN 0025-5408, URL https://www.sciencedirect.com/science/article/pii/0025540883901381.

[5] M. Thackeray, P. Johnson, L. de Picciotto, P. Bruce, and J. Goodenough, Materials Research Bulletin **19**, 179 (1984), ISSN 0025-5408, URL https://www.sciencedirect.com/science/article/pii/0025540884900886.

[6] M. M. Thackeray, S.-H. Kang, C. S. Johnson, J. T. Vaughey, R. Benedek, and S. A. Hackney, J. Mater. Chem. **17**, 3112 (2007), URL http://dx.doi.org/10.1039/B702425H.

[7] M. Freire, N. V. Kosova, C. Jordy, D. Chateigner, O. I. Lebedev, A. Maignan, and V. Pralong, Nature Materials **15**, 173 (2016), ISSN 1476-4660, URL https://doi.org/10.1038/nmat4479.

[8] A. Chakraborty, S. Kunnikuruvan, S. Kumar, B. Markovsky, D. Aurbach, M. Dixit, and D. T. Major, Chemistry of Materials **32**, 915 (2020), ISSN 0897-4756, URL https://doi.org/10.1021/acs.chemmater.9b04066.

[9] I. D. Seymour, S. Chakraborty, D. S. Middlemiss, D. J. Wales, and C. P. Grey, Chemistry of Materials **27**, 5550 (2015), ISSN 0897-4756, URL https://doi.org/10.1021/acs.chemmater.5b01674.

[10] I. D. Seymour, D. J. Wales, and C. P. Grey, The Journal of Physical Chemistry C **120**, 19521 (2016), ISSN 1932-7447, URL https://doi.org/10.1021/acs.jpcc.6b05307.

[11] Y. Zhang, H. Xie, H. Jin, Q. Zhang, Y. Li, X. Li, K. Li, and C. Bao, IOP Conference Series: Earth and Environmental Science **603**, 012051 (2020), URL https://doi.org/10.1088/1755-1315/603/1/012051.

[12] J. Greedan, N. Raju, and I. Davidson, Journal of Solid State Chemistry **128**, 209 (1997), ISSN 0022-4596, URL https://www.sciencedirect.com/science/article/pii/S0022459696971893.

[13] T. Ohzuku, A. Ueda, and M. Nagayama, Journal of The Electrochemical Society **140**, 1862 (1993), URL https://doi.org/10.1149/1.2220730.

[14] J. R. Dahn, U. von Sacken, M. W. Juzkow, and H. Al-Janaby, Journal of The Electrochemical Society **138**, 2207 (1991), URL https://doi.org/10.1149/1.2085950.

[15] M. Broussely, F. Perton, P. Biensan, J. Bodet, J. Labat, A. Lecerf, C. Delmas, A. Rougier, and J. Pérès, Journal of Power Sources **54**, 109 (1995), ISSN 0378-7753, proceedings of the Seventh International Meeting on Lithium Batteries, URL https://www.sciencedirect.com/science/article/pii/0378775394020499.

[16] T. Ohzuku and Y. Makimura, Chemistry Letters **30**, 642 (2001), https://doi.org/10.1246/cl.2001.642, URL https://doi.org/10.1246/cl.2001.642.

[17] N. Yabuuchi and T. Ohzuku, Journal of Power Sources **119-121**, 171 (2003), ISSN 0378-7753, selected papers presented at the 11th International Meeting on Lithium Batteries, URL https://www.sciencedirect.com/science/article/pii/S0378775303001733.

[18] C. Xu, K. Märker, J. Lee, A. Mahadevegowda, P. J. Reeves, S. J. Day, M. F. Groh, S. P. Emge, C. Ducati, B. Layla Mehdi, et al., Nature Materials **20**, 84 (2021), ISSN 1476-4660, URL https://doi.org/10.1038/s41563-020-0767-8.

[19] C. Xu, P. J. Reeves, Q. Jacquet, and C. P. Grey, Advanced Energy Materials **11**, 2003404 (2021), https://onlinelibrary.wiley.com/doi/pdf/10.1002/aenm.202003404, URL https://onlinelibrary.wiley.com/doi/abs/10.1002/aenm.202003404.

[20] C. Julien, A. Mauger, K. Zaghib, and H. Groult, Materials **9** (2016), ISSN 1996-1944, URL https://www.mdpi.com/1996-1944/9/7/595.

[21] A. K. Stephan, Joule **4**, 1632 (2020), ISSN 2542-4351, URL https://www.sciencedirect.com/science/article/pii/S2542435120303500.

[22] M. Tabuchi, K. Ado, H. Kobayashi, H. Kageyama, C. Masquelier, A. Kondo, and R. Kanno, Journal of The Electrochemical Society **145**, L49 (1998), URL https://doi.org/10.1149/1.1838411.

[23] Y. Shao-Horn, S. A. Hackney, A. R. Armstrong, P. G. Bruce, R. Gitzendanner, C. S. Johnson, and M. M. Thackeray, Journal of The Electrochemical Society **146**, 2404 (1999), URL https://doi.org/10.1149/1.1391949.

[24] J. Reed, G. Ceder, and A. V. D. Ven, Electrochemical and Solid-State Letters **4**, A78 (2001), URL https://doi.org/10.1149/1.1368896.

[25] A. R. Armstrong, N. Dupre, A. J. Paterson, C. P. Grey, and P. G. Bruce, Chemistry of Materials **16**, 3106 (2004), ISSN 0897-4756, URL https://doi.org/10.1021/cm034964b.

[26] S. Kim, X. Ma, S. P. Ong, and G. Ceder, Phys. Chem. Chem. Phys. **14**, 15571 (2012), URL http://dx.doi.

org/10.1039/C2CP43377J.
[27] J. N. Reimers and J. R. Dahn, Journal of The Electrochemical Society **139**, 2091 (1992), URL https://doi.org/10.1149/1.2221184.
[28] T. Ohzuku and A. Ueda, Journal of The Electrochemical Society **141**, 2972 (1994), URL https://doi.org/10.1149/1.2059267.
[29] G. G. Amatucci, J. M. Tarascon, and L. C. Klein, Journal of The Electrochemical Society **143**, 1114 (1996), URL https://doi.org/10.1149/1.1836594.
[30] M. Ménétrier, I. Saadoune, S. Levasseur, and C. Delmas, J. Mater. Chem. **9**, 1135 (1999), URL http://dx.doi.org/10.1039/A900016J.
[31] E. Flores, N. Mozhzhukhina, U. Aschauer, and E. J. Berg, ACS Applied Materials & Interfaces **13**, 22540 (2021), pMID: 33947179, https://doi.org/10.1021/acsami.1c04383, URL https://doi.org/10.1021/acsami.1c04383.
[32] A. J. Merryweather, C. Schnedermann, Q. Jacquet, C. P. Grey, and A. Rao, Nature **594**, 522 (2021), ISSN 1476-4687, URL https://doi.org/10.1038/s41586-021-03584-2.
[33] M. D. Radin, S. Hy, M. Sina, C. Fang, H. Liu, J. Vinckeviciute, M. Zhang, M. S. Whittingham, Y. S. Meng, and A. Van der Ven, Advanced Energy Materials **7**, 1602888 (2017), https://onlinelibrary.wiley.com/doi/pdf/10.1002/aenm.201602888, URL https://onlinelibrary.wiley.com/doi/abs/10.1002/aenm.201602888.
[34] P. Werner and A. J. Millis, Phys. Rev. B **75**, 085108 (2007), URL https://link.aps.org/doi/10.1103/PhysRevB.75.085108.
[35] A. Liebsch, Phys. Rev. B **77**, 115115 (2008), URL https://link.aps.org/doi/10.1103/PhysRevB.77.115115.
[36] E. Gati, U. Tutsch, A. Naji, M. Garst, S. Köhler, H. Schubert, T. Sasaki, and M. Lang, Crystals **8** (2018), ISSN 2073-4352, URL https://www.mdpi.com/2073-4352/8/1/38.
[37] J. F. Oliveira, M. B. Fontes, M. Moutinho, S. E. Rowley, E. Baggio-Saitovitch, M. B. Silva Neto, and C. Enderlein, Communications Materials **2**, 1 (2021), ISSN 2662-4443, URL https://doi.org/10.1038/s43246-020-00110-1.
[38] C. A. Marianetti, G. Kotliar, and G. Ceder, Nature Materials **3**, 627 (2004), ISSN 1476-4660, URL https://doi.org/10.1038/nmat1178.
[39] A. Georges and G. Kotliar, Phys. Rev. B **45**, 6479 (1992), URL https://link.aps.org/doi/10.1103/PhysRevB.45.6479.
[40] A. Georges, G. Kotliar, W. Krauth, and M. J. Rozenberg, Rev. Mod. Phys. **68**, 13 (1996), URL https://link.aps.org/doi/10.1103/RevModPhys.68.13.
[41] D. Vollhardt, Annalen der Physik **524**, 1 (2012), https://onlinelibrary.wiley.com/doi/pdf/10.1002/andp.201100250, URL https://onlinelibrary.wiley.com/doi/abs/10.1002/andp.201100250.
[42] A. Georges, AIP Conference Proceedings **715**, 3 (2004), https://aip.scitation.org/doi/pdf/10.1063/1.1800733, URL https://aip.scitation.org/doi/abs/10.1063/1.1800733.
[43] G. Kotliar, S. Y. Savrasov, K. Haule, V. S. Oudovenko, O. Parcollet, and C. A. Marianetti, Rev. Mod. Phys. **78**, 865 (2006), URL https://link.aps.org/doi/10.1103/RevModPhys.78.865.
[44] K. Held, Advances in Physics **56**, 829 (2007), https://doi.org/10.1080/00018730701619647, URL https://doi.org/10.1080/00018730701619647.
[45] E. B. Isaacs and C. A. Marianetti, Phys. Rev. B **102**, 045146 (2020), URL https://link.aps.org/doi/10.1103/PhysRevB.102.045146.
[46] W. H. Sio, C. Verdi, S. Poncé, and F. Giustino, Phys. Rev. B **99**, 235139 (2019), URL https://link.aps.org/doi/10.1103/PhysRevB.99.235139.
[47] W. H. Sio, C. Verdi, S. Poncé, and F. Giustino, Phys. Rev. Lett. **122**, 246403 (2019), URL https://link.aps.org/doi/10.1103/PhysRevLett.122.246403.
[48] X. Li, Z. Su, and Y. Wang, Journal of Alloys and Compounds **735**, 2182 (2018), ISSN 0925-8388, URL https://www.sciencedirect.com/science/article/pii/S092583881734166X.
[49] V. Galakhov, M. Korotin, N. Ovechkina, E. Kurmaev, V. Gorshkov, D. Kellerman, S. Bartkowski, and M. Neumann, **14**, 281 – 286 (2000), URL https://www.scopus.com/inward/record.uri?eid=2-s2.0-0008802115&doi=10.1007%2fs100510050130&partnerID=40&md5=d7dab932ff51b8178c3d33615d882d76.
[50] D. J. Singh, Phys. Rev. B **55**, 309 (1997), URL https://link.aps.org/doi/10.1103/PhysRevB.55.309.
[51] N. Nath Shukla and R. Prasad, Journal of Physics and Chemistry of Solids **67**, 1731 (2006), ISSN 0022-3697, URL https://www.sciencedirect.com/science/article/pii/S0022369706002290.
[52] S. K. Mishra and G. Ceder, Phys. Rev. B **59**, 6120 (1999), URL https://link.aps.org/doi/10.1103/PhysRevB.59.6120.
[53] M. Tuccillo, O. Palumbo, M. Pavone, A. B. Muñoz-García, A. Paolone, and S. Brutti, Crystals **10** (2020), ISSN 2073-4352, URL https://www.mdpi.com/2073-4352/10/6/526.
[54] H. Banerjee, H. Schnait, M. Aichhorn, and T. Saha-Dasgupta, Phys. Rev. B **105**, 235106 (2022), URL https://link.aps.org/doi/10.1103/PhysRevB.105.235106.
[55] P. Wissgott, A. Toschi, H. Usui, K. Kuroki, and K. Held, Phys. Rev. B **82**, 201106 (2010), URL https://link.aps.org/doi/10.1103/PhysRevB.82.201106.
[56] Y.-F. Yang and K. Held, Phys. Rev. B **76**, 212401 (2007), URL https://link.aps.org/doi/10.1103/PhysRevB.76.212401.
[57] H. Banerjee, O. Janson, K. Held, and T. Saha-Dasgupta, Phys. Rev. B **100**, 115143 (2019), URL https://link.aps.org/doi/10.1103/PhysRevB.100.115143.
[58] H. Banerjee and M. Aichhorn, Phys. Rev. B **101**, 241112 (2020), URL https://link.aps.org/doi/10.1103/PhysRevB.101.241112.
[59] J. H. Lee, K. T. Delaney, E. Bousquet, N. A. Spaldin, and K. M. Rabe, Phys. Rev. B **88**, 174426 (2013), URL https://link.aps.org/doi/10.1103/PhysRevB.88.174426.